Raman Interferometry between Autoionizing States to Probe Ultrafast Wave-Packet Dynamics with High Spectral Resolution

A. Plunkett,[1] M. A. Alarcón,[2] J. K. Wood,[3] C. H. Greene,[2] and A. Sandhu[1,3,*]
[1]Department of Physics, University of Arizona, Tucson, Arizona 85721, USA
[2]Department of Physics and Astronomy, Purdue University, West Lafayette, Indiana 47907, USA
[3]College of Optical Sciences, University of Arizona, Tucson, Arizona 85721, USA

(Received 6 November 2021; accepted 25 January 2022; published 22 February 2022)

Photoelectron interferometry with femtosecond and attosecond light pulses is a powerful probe of the fast electron wave-packet dynamics, albeit it has practical limitations on the energy resolution. We show that one can simultaneously obtain both high temporal and spectral resolution by stimulating Raman interferences with one light pulse and monitoring the modification of the electron yield in a separate step. Applying this spectroscopic approach to the autoionizing states of argon, we experimentally resolved its electronic composition and time evolution in exquisite detail. Theoretical calculations show remarkable agreement with the observations and shed light on the light-matter interaction parameters. Using appropriate Raman probing and delayed detection steps, this technique enables highly sensitive probing and control of electron dynamics in complex systems.

DOI: 10.1103/PhysRevLett.128.083001

Photoelectron wave-packet interferometry has been extensively applied to probe the electronic properties of atoms and molecules, to characterize the amplitudes and phases of constituent wave functions [1–6], and probe the strong field dynamics [7–9], autoionization [10–12], correlated electron dynamics [13–15], and molecular dynamics [16]. Typically, a bound atomic or molecular wave packet can be prepared by exciting the system with a broadband femtosecond or attosecond pulse, followed by a delayed ionizing probe light pulse that interferes with various components of the wave packet in the continuum. The interference pattern can be resolved in kinetic energy, and its evolution exhibits quantum beating in time delay due to the phase differences between the states. Beat frequencies obtained from the Fourier analysis of the signal can then be used to deduce information about the composition of the wave packet. However, the beat frequency resolution is constrained by the practical limitations on the time-delay range that can be explored in a typical experiment. On the other hand, electron kinetic energy resolution is constrained by the probe pulse duration. These issues limit the amount of information that can be extracted from spectrograms, especially when dealing with a multitude of states with unknown energies and potentially overlapping beat frequencies.

We introduce an alternate approach, which employs impulsive stimulated Raman interferences, followed by a deferred detection, to investigate the electron dynamics with both high temporal *and* spectral resolution. After an excited wave packet is prepared, a time-delayed Raman probe pulse redistributes the wave-packet amplitudes, setting up a delay-dependent quantum interferences in the bound or metastable state manifold, allowing femtosecond-resolved probing and control of the electron dynamics. For the actual electron signal acquisition, we rely on a deferred detection through the natural decay of the electronic states or by using a separate narrow-band ionization pulse. This long-timescale detection provides the high energy resolution, enabling the direct identification of the electronic constituents of the wave packet. Furthermore, we achieve high sensitivity by analyzing the changes in the electron spectra, i.e., by extracting the Raman probe induced modification of the signal. Combination of these advances can enable new insights into the electronic structure and quantum dynamics in atoms and molecules, while also elucidating the nature of light-induced couplings in exquisite detail.

To demonstrate the power of this technique we apply it to investigate a wave packet composed of the autoionizing states of argon, as illustrated in Fig. 1. Argon ion features a spin-orbit splitting of 180 meV, with the $(^2P_{3/2})$ ground state and $(^2P_{1/2})$ excited state lying 15.76 eV and 15.94 eV above the neutral ground state, respectively [17]. Between these two thresholds, electrons exist autoionizing resonances where the Rydberg electron is attached to an "ion-core" state $^2P_{1/2}$. A two-color pump consisting of a few-fs extreme ultraviolet (EUV) emission centered at 14.3 eV and a 40 fs near-infrared (NIR) pulse centered at 1.6 eV was used to coherently launch an "optically dark" autoionizing nf' $(n \geq 9)$ wave packet within this argon spin orbit–excited manifold. A time-delayed ~60 fs (FWHM), short-wave-infrared (SWIR) probe centered at 1 eV is used to induce Raman transitions between the constituents of the

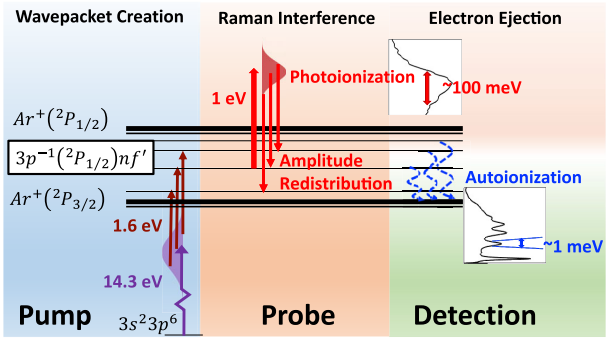

FIG. 1. Two-color (EUV + NIR) "pump" pulse excites an nf' autoionizing wave packet in the argon atom. A time-delayed femtosecond SWIR "probe" pulse induces impulsive Raman transitions between the constituents of the wave packet, redistributing the population within the wave packet. Electronic states undergo slow autoionization producing sharp features in the electron spectra. Analysis of changes in the spectra of this delayed signal as function of pump-probe delay provides both time and energy resolution.

wave packet. Because of multielectron interactions, the states relax via autoionization, simultaneously releasing the Rydberg electron and rearranging the core state to the lower-energy spin-orbit configuration $3s^23p^5(^2P_{1/2})nl \rightarrow 3s^23p^5(^2P_{3/2}) + e^-$. This natural autoionization decay, which produces sharp electron peaks between 40 and 150 meV [18], is used as detection channel. The population redistribution by the Raman probe causes energy-dependent positive and negative changes in the electron yield, which can be detected by subtracting the spectra obtained with and without SWIR Raman probe. Fourier analysis of the energy resolved delay-dependent signals allows us to unambiguously determine the constituent states of the wave packet even when the beat frequencies are overlapping.

To obtain the light pulses, we employed a Ti:Sapphire 780 nm NIR laser amplifier with 2 mJ pulse energy, 40 fs pulse duration. Half of the NIR pulse energy drives the EUV generation in a xenon filled gas cell producing harmonics 9–17th. EUV pulse and the copropagating NIR driver were focused onto an effusive argon jet with a toroidal mirror. The 9th harmonic plus NIR path dominates the excitation of nf' states, with a combined bandwidth of ~180 meV. The other half of the NIR pulse from the amplifier was used to produce a 60 fs, 1240 nm SWIR pulse with an optical parametric amplifier. Using a 50 cm lens, the SWIR pulse was focused to an intensity of ~1 TW/cm^2 on the argon target. The pump (EUV + NIR) and time-delayed probe (SWIR) were collinearly recombined on a mirror with a hole before the target chamber. The photoelectrons and autoionization electrons were acquired using a velocity map imaging spectrometer [9,19], and the difference in spectra with and without SWIR probe is analyzed as a function of the probe time delay.

Tools from multichannel quantum defect theory (MQDT) and second order time-dependent perturbation theory are used to model the light-matter interaction. Assuming that only the outer electron interacts with the field, the two-color (pump) excitation proceeds through an intermediate $3d'$ state viewed as purely attached to the $3s^23p^5(^2P_{1/2})$ ionic core. This restricts the space of possible states that form the wave packet to bound states with total $J = 0$ or $J = 2$, i.e., an ionic core in state $3s^23p^5(^2P_{1/2})$ and an outer electron with orbital angular momentum equal to $\ell = 1$ or $\ell = 3$. Using the MQDT parameters from Pellarin *et al.* [20] we determined the width and position of the autoionizing resonances with total $J = 2$ for both p' and f' states [21,22]. Because the f' states dominate by approximately 2 orders of magnitude, the p' autoionizing Rydberg states are neglected.

As in [23] the wave packet is described by an integral over energy, and a sum over the open channels and allowed symmetries. Since the excitation probability is highly concentrated around the narrow f' resonances, an approximate wave packet is obtained by summing over the countable resonances

$$|\Psi_o\rangle = \mathcal{A}\sum_n A_n|\psi_n\rangle = \mathcal{A}\sum_n A_n \frac{u_{n,3}(r)}{r}\Phi^{J=2}_{1/2}, \quad (1)$$

where $\Phi^{J=2}_{j_c} = \chi_{j_c}|\{[(\ell_c, s_c)j_c, s]J_{cs}, \ell\}J, M\rangle$ is the J_{cs} coupled angular momentum state [24], with an ionic core of angular momentum j_c and total angular momentum J. $\mathcal{A}$ is the antisymmetrization operator.

The radial part of the wave function $u_{n,3}(r)$ is approximated here by a hydrogenic orbital rather than by a Whittaker function, since nf'-state quantum defects are small. Our treatment considers only the $J = 2$ functions with $j_c = 1/2$ and $\ell = 3$, giving $J_{cs} = 1$. The dependence of A_n on n reflects the characteristics of the driver laser, with an assumed Gaussian spectral profile.

The probability amplitude for each autoionizing state in the wave packet upon interaction with the delayed SWIR pulse is based on the perturbative expansion of the transition operator, as in Chap. 2 of [25]. The first nonvanishing contribution comes from the second order term, corresponding to a two photon Raman process.

For a laser pulse with field strength $\mathcal{E}_o$, central frequency ω, polarization $\hat{\epsilon}$, time delay t_o, and temporal FWHM $2\sigma\ln 2$, the time-dependent perturbation is

$$V(t) = \mathcal{E}_o e^{-[(t-t_o)/\sigma]^2}\cos(\omega t)\hat{\epsilon}\cdot\vec{r} \quad (2)$$

in the length gauge. With this perturbation, the second order transition matrix element between the initial wave packet and one of the Rydberg states has the form

$$\langle\psi_f|T^{(2)}|\Psi_o\rangle = -\mathcal{E}_o^2\sum_n T_{f,n}e^{-i(E_f-E_n)t_o-\frac{\Gamma_f+\Gamma_n}{2}t_o}, \quad (3)$$

where $E_n(E_f)$ is the energy and $\Gamma_n(\Gamma_f)$ is the autoionization width of the initial (final) Rydberg state.

The amplitude $T^{(2)}_{f,n}$ involves a sum and integral over intermediate states of the dipole matrix elements multiplied by the spectral profile of the laser evaluated at the photon energies for the Raman transition. The sum of zeroth and second order transition matrix elements gives the combined amplitude for the final Rydberg state f:

$$\langle\psi_f|T|\Psi_o\rangle = A_f + \langle\psi_f|T^{(2)}|\Psi_o\rangle. \tag{4}$$

The modification of electron yield for autoionization of state $|\psi_f\rangle$ is obtained by taking the difference between the probability of a two photon transition and the initial probability in state $|\psi_f\rangle$. For initially populated states this is second order in the SWIR field strength:

$$D(f,t_o) = -\mathcal{E}_o^2 2\Re A_f^*\langle\psi_f|T^{(2)}|\Psi_o\rangle + O(\mathcal{E}_o^4). \tag{5}$$

Notice that even if the interaction with the intermediate states allows, in principle, for the excitation of nf' states with different J and M values, as well as the excitation of the np' autoionizing states, their contributions are too weak to be observed in the experiment. Also, the difference signal is due to the interference between the initially populated states *only*. The depletion and enhancement is thus polarized in the direction of pump pulse, irrespective of the Raman probe polarization.

Figure 2(a) shows the traditional photoelectron spectrogram resulting from ionization of nf' wave packet with the femtosecond SWIR probe, which interrupts the autoionization. The electron kinetic energy is along the vertical axis and pump-probe time delay along the horizontal axis. For the 1 eV SWIR probe, the electron kinetic energy lies between 0.8 and 1 eV. Because of the broad bandwidth of the probe pulse, the photoionization amplitudes from different states composing the wave packet can interfere in the continuum and lead to beating as a function of pump-probe delay. The beat frequencies depend on the energy separation between constituent states, but there is no state-resolved information along the kinetic energy axis. The spectral smearing, and therefore loss of kinetic energy resolution, is a necessary feature of such experiments since, without it, there would be no interference.

In contrast, Fig. 2(b) shows the experimental results obtained using our Raman interferometry approach, where we monitor the modification of the autoionization spectra due to the coherent redistribution of the wave-packet amplitudes by the probe pulse. For the nf' states, autoionized electrons emerge with between 0 and 180 meV of kinetic energy, and these states have ≈10–1000 ps lifetimes. The deferred detection inherent in this method yields impressive kinetic energy resolution, and we can monitor the quantum beating at specific electronic binding energies of the system. For example, the lowest kinetic energy

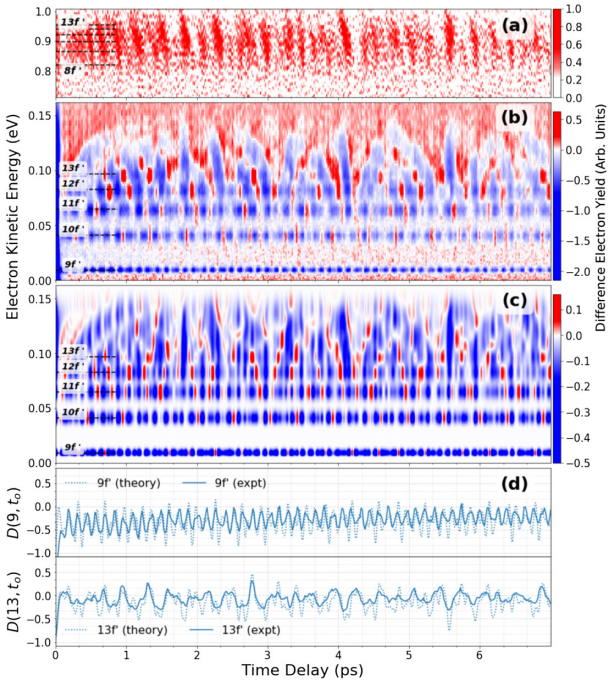

FIG. 2. Experimental difference electron spectrograms corresponding to (a) photoionization and (b) autoionization. (c) Theoretical results for the autoionization. The photoionization exhibits beats due to the interferences between different nf' ionization paths, but there is loss of resolution along the kinetic energy axis due to the probe bandwidth. The autoionization yield is modulated by the coherent Raman redistribution induced by the probe. The detection following long autoionization timescales provides excellent resolution in electronic binding energies, allowing much better analysis of the beats and wave-packet evolution. (d) Lineouts from (b) and (c) to quantitatively compare experimental and theoretical beat evolution at $9f'$ and $13f'$ states.

feature, corresponding to $9f'$ state, shows a faster oscillation due to larger spacing between the lower n Rydberg levels.

Another important feature of this experiment is that it demonstrates coherent control of the wave packet. Note that the blue color in Fig. 2(b) implies reduction in the autoionization probability compared with initial value, whereas the red color implies enhancement of the autoionization yield at that specific energy, which is a direct evidence of the time-dependent redistribution of electronic probability by a Raman process.

Figure 2(c) shows the calculated difference electron spectrogram for parameters identical to the experiment. The agreement between experiment and theory is remarkable, showing that the model captures the detailed evolution of the wave-packet dynamics as well as the light-induced enhancement of specific wave-packet components. Figure 2(d) shows the lineouts of difference electron yield at kinetic energies corresponding to the $9f'$ and $13f'$ states, to quantify the experiment-theory agreement.

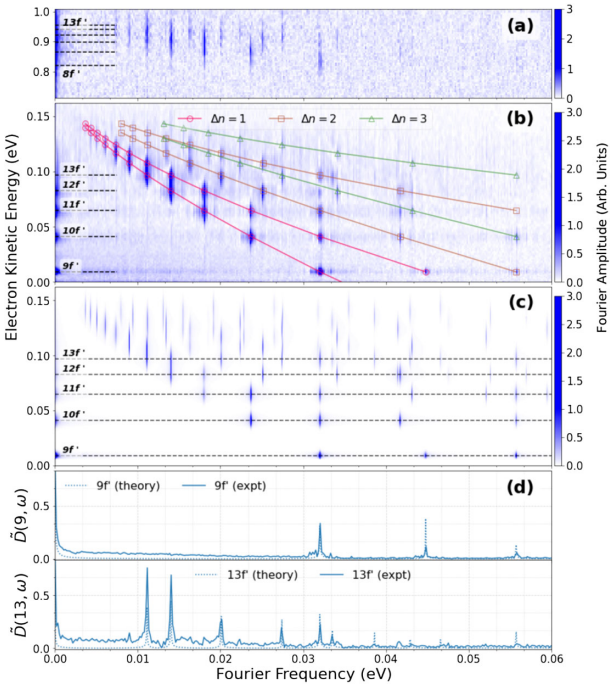

FIG. 3. Fourier spectrogram of the (a) experimental photoionization signal, (b) autoionization signal, and (c) autoionization theory. The Fourier frequencies corresponding to the energy differences between nf' states appear on the horizontal axis, while peaks corresponding to the electron binding energies are visible along the vertical axis. Photoionization results do not identify specific states unambiguously, whereas the difference autoionization signals from the Raman probing allow the investigation of electronic composition in detail. Overlaid curves represent the expected position of the beats for pairs of states separated by $\Delta n = \pm 1, 2, 3$. (d) Lineouts from (b) and (c) to quantitatively compare experimental and theoretical beat strengths at $9f'$ and $13f'$ energies.

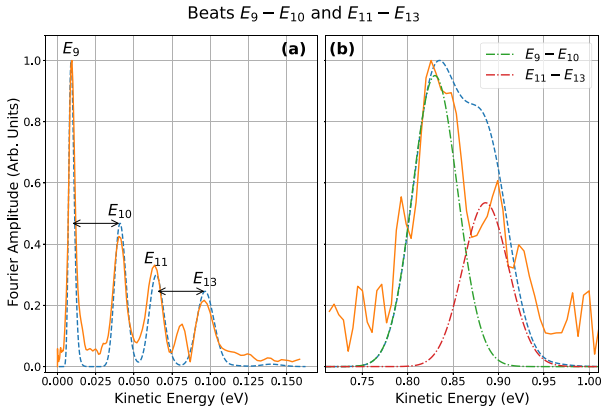

FIG. 4. (a) Kinetic energy resolved amplitude of difference autoionization signal in experiment (solid line) and theory (dashed line) differentiates two beat pairs, between states $9f'$ and $10f'$ and states $11f'$ and $13f'$, that lie in the same beat frequency bin and otherwise would be nonseparable. (b) Photoionization spectra do not have the kinetic energy resolution to distinguish the overlapping contributions in experiment (solid line) or theory (dashed line). Calculated photoionization amplitude for each beat pair is shown (dot-dashed line).

Figure 3 shows the Fourier transform of the time evolution reported in Fig. 2. Figure 3(a) again refers to direct interferences in the higher energy continuum due to photoionization by the femtosecond probe pulse. One can see quantum beats due to energy separations between the states. However, due to kinetic energy smearing by the broadband probe, one cannot determine the binding energies or separate nearby beats. In contrast, the difference autoionization signal in Fig. 3(b) exhibits superb resolution along the kinetic energy axis limited only by the instrumental resolution. We can clearly identify the electronic states along the vertical axis ordered by the quantum number from $9f'$ onward. It is also easy to observe that several beat frequencies on the horizontal axis correspond to more than one pair of states interfering with each other. The curves overlaid on Fig. 3(b) identify the beats corresponding to principle quantum number differences $\Delta n = \pm 1, 2, 3$. The high frequency beats, absent in direct photoionization, are prominently visible here due to better sensitivity. The theoretical result in Fig. 3(c) captures the experimental detail in terms of both the beat frequencies and kinetic energies. This agreement allows us to quantify the electronic properties of autoionizing states and demonstrates the benefits of our approach over direct photoelectron interferometry.

Figure 4 provides specific examples of the advantage of our method. Figure 4(a) shows kinetic energy resolved Fourier amplitudes extracted from Fig. 3 at the beat frequency 0.032 eV. The plot clearly identifies the participating electronic states and demonstrates that our narrow frequency bin actually contains two pairs of beats, $E_9 - E_{10}$ and $E_{11} - E_{13}$, separated only by ~ 2 μeV, which otherwise would be indistinguishable due to the limitation on the Fourier frequency resolution. Note that the small peak at 0.08 eV corresponds to the state $12f'$, since beat $E_{12} - E_{15}$ also falls in the same frequency bin for the experimental data. Figure 4(b) shows the kinetic energy resolved Fourier amplitude at the same beat frequency, but in the photoionization energy region. Clearly, one cannot distinguish specific contributions from the experimental data due to the lack of kinetic energy resolution and poor signal to noise. Thus, the assignment of states in this case is impractical with conventional photoelectron interferometry. Even the theoretical plot for the photoionization cannot unambiguously resolve the two beat contributions. Because of the finite bandwidth of the laser, a single broad peak results from the overlap of the photoionization amplitudes of two pairs of states. The amplitude for each beat pair is centered around the average energy for the pair, as shown by the dot-dashed lines.

This experiment showcases the ability to conduct a femtosecond study with a very high energy resolution, where we clearly distinguish the electronic states that otherwise would have produced overlapping beats in the Fourier spectrum of a traditional photoelectron signal. By using a tailored Raman probe, one can also exert coherent control to create the desired wave packets. The essence of our technique lies in the separation of temporal probing and energy measurement steps, thus circumventing the uncertainty principle. Using shortest excitation and Raman pulses one can achieve few-femtosecond time resolution. The energy is independently measured via delayed detection. For naturally decaying states, the relaxation time governs the energy resolution. In the case of bound states, one can employ a separate quasimonochromatic pulse for ionization, where the energy resolution is limited only by the practical need for intense narrow-band pulses and the instrumental resolution. Our approach can be applied to the excited molecular wave packets that usually form a dense manifold of states, providing a powerful tool to analyze the time evolution and electronic structure of complex systems.

A. P., J. W., and A. S. acknowledge support from the National Science Foundation under Grants No. PHY 1912455 and No. PHY 1919486. M. A. and C. H. G. acknowledge support from the U.S. Department of Energy, Office of Science, Office of Basic Energy Sciences, under Award No. DE-SC0010545.

*Corresponding author.
asandhu@arizona.edu

[1] T. Remetter, P. Johnsson, J. Mauritsson, K. Varju, Y Ni, F. Lepine, E. Gustafsson, M. Kling, J. Khan, R. Lopez-Martens, K. J. Schafer, M. J. J. Vrakking, and A. L'Huillier, Attosecond electron wave packet interferometry, Nat. Phys. **2**, 323 (2006).

[2] K. Klünder, P. Johnsson, M. Swoboda, A. L'Huillier, G. Sansone, M. Nisoli, M. J. J. Vrakking, K. J. Schafer, and J. Mauritsson, Reconstruction of attosecond electron wave packets using quantum state holography, Phys. Rev. A **88**, 033404 (2013).

[3] C. Liu and M. Nisoli, Attosecond electron interferometry for measurement of the quantum phase of free-electron wave packets, Phys. Rev. A **86**, 053404 (2012).

[4] M. Han, P. Ge, Y. Shao, Q. Gong, and Y. Liu, Attoclock Photoelectron Interferometry with Two-Color Corotating Circular Fields to Probe the Phase and the Amplitude of Emitting Wave Packets, Phys. Rev. Lett. **120**, 073202 (2018).

[5] R. Forbes, V. Makhija, J. G. Underwood, A. Stolow, I. Wilkinson, P. Hockett, and R. Lausten, Quantum-beat photoelectron-imaging spectroscopy of Xe in the VUV, Phys. Rev. A **97**, 063417 (2018).

[6] L. D. Noordam and R. R. Jones, Probing Rydberg electron dynamics, J. Mod. Opt. **44**, 2515 (1997).

[7] M. Li, Hui Xie, W. Cao, S. Luo, J. Tan, Y. Feng, B. Du, W. Zhang, Y. Li, Q. Zhang, P. Lan, Y. Zhou, and P. Lu, Photoelectron Holographic Interferometry to Probe the Longitudinal Momentum Offset at the Tunnel Exit, Phys. Rev. Lett. **122**, 183202 (2019).

[8] D. M. Villeneuve, P. Hockett, M. J. J. Vrakking, and H. Niikura, Coherent imaging of an attosecond electron wave packet, Science **356**, 1150 (2017).

[9] N. Shivaram, H. Timmers, X.-M. Tong, and A. Sandhu, Attosecond-Resolved Evolution of a Laser-Dressed Helium Atom: Interfering Excitation Paths and Quantum Phases, Phys. Rev. Lett. **108**, 193002 (2012).

[10] D. Busto, L. Barreau, M. Isinger, M. Turconi, C. Alexandridi, A. Harth, S. Zhong, R. J. Squibb, D. Kroon, S. Plogmaker, M. Miranda, A. Jiménez-Galán, L. Argenti, C. L. Arnold, R. Feifel, F. Martín, M. Gisselbrecht, A. L'Huillier, and P. Salières, Time-frequency representation of autoionization dynamics in helium, J. Phys. B **51**, 044002 (2018).

[11] V. Gruson, L. Barreau, A. Jiménez-Galan, F. Risoud, J. Caillat, A. Maquet, B. Carré, F. Lepetit, J. F. Hergott, T. Ruchon, L. Argenti, R. Taïeb, F. Martín, and P. Salières, Attosecond dynamics through a Fano resonance: Monitoring the birth of a photoelectron, Science **354**, 734 (2016).

[12] J. A. Ramswell, V. G. Stavros, Q. Hong, and H. H. Fielding, Rydberg electron wavepacket dynamics in atoms and molecules, Phil. Trans. R. Soc. A **356**, 363 (1998).

[13] E. P. Månsson, D. Guénot, C. L. Arnold, D. Kroon, S. Kasper, J. Marcus Dahlström, E. Lindroth, A. S. Kheifets, A. L'Huillier, S. L. Sorensen, and M. Gisselbrecht, Double ionization probed on the attosecond timescale, Nat. Phys. **10**, 207 (2014).

[14] S. Usenko *et al.*, Auger electron wave packet interferometry on extreme timescales with coherent soft x-rays, J. Phys. B **53**, 244008 (2020).

[15] J. Feist, S. Nagele, C. Ticknor, B. I. Schneider, L. A. Collins, and J. Burgdörfer, Attosecond Two-Photon Interferometry for Doubly Excited States of Helium, Phys. Rev. Lett. **107**, 093005 (2011).

[16] A. González-Castrillo, F. Martín, and A. Palacios, Quantum state holography to reconstruct the molecular wave packet using an attosecond XUV-XUV pump-probe technique, Sci. Rep. **10**, 12981 (2020).

[17] A. Kramida, Yu. Ralchenko, J. Reader (NIST ASD Team), NIST Atomic Spectra Database (ver. 5.7.1) [Online], Available: https://physics.nist.gov/asd [2020, August 24], National Institute of Standards and Technology, Gaithersburg, MD. (2019).

[18] Y. Y. Lee, T. Y. Dung, R. M. Hsieh, J. Y. Yu, Y. F. Song, G. H. Ho, T. P. Huang, W. C. Pan, I. Chia, S. Y. Tu, A. H. Kung, and L. C. Lee, Autoionizing Rydberg series (np', nf') of Ar investigated by stepwise excitations with lasers and synchrotron radiation, Phys. Rev. A **78**, 022509 (2008).

[19] A. Plunkett, N. Harkema, R. R. Lucchese, C. W. McCurdy, and A. Sandhu, Ultrafast Rydberg-state dissociation in oxygen: Identifying the role of multielectron excitations, Phys. Rev. A **99**, 063403 (2019).

[20] M. Pellarin, J. L. Vialle, M. Carré, J. Lermé, and M. Aymar, Even parity series of argon Rydberg states studied by

fast-beam collinear laser spectroscopy, J. Phys. B **21**, 3833 (1988).

[21] M. Aymar, C. H. Greene, and E. Luc-Koenig, Multichannel Rydberg spectroscopy of complex atoms, Rev. Mod. Phys. **68**, 1015 (1996).

[22] M. J. Seaton, Quantum Defect Theory, Rep. Prog. Phys. **46**, 167 (1983).

[23] F. Robicheaux and W. T. Hill, Autoionizing Rydberg wave packets, Phys. Rev. A **54**, 3276 (1996).

[24] M. D. Lindsay, C. J. Dai, L. T. Cai, T. F. Gallagher, F. Robicheaux, and C. H. Greene, Angular-distributions of ejected electrons from autoionizing 3pnd states of magnesium, Phys. Rev. A **46**, 3789 (1992).

[25] F. H. M. Faisal, *Theory of Multiphoton Processes* (Springer, US, 1987).